Environmental Science & Technology

pubs.acs.org/est

Article

Modulating the Activity and SO_2 Resistance of α-Fe_2O_3 Catalysts for NH_3−SCR of NO_x via Crystal Facet Engineering

Siqing Cheng,[§] Fang Xu,[§] Shan Yang, Bifeng Zhang, Wang Song, Xuechen Zhu, Wei Tan,* Chuanzhi Sun,* and Lin Dong

Cite This: *Environ. Sci. Technol.* 2024, 58, 8955−8965

Read Online

ACCESS | Metrics & More | Article Recommendations | Supporting Information

ABSTRACT: The development of Fe-based catalysts for the selective catalytic reduction of NO_x by NH_3 (NH_3−SCR of NO_x) has garnered significant attention due to their exceptional SO_2 resistance. However, the influence of different sulfur-containing species (e.g., ferric sulfates and ammonium sulfates) on the NH_3−SCR activity of Fe-based catalysts as well as its dependence on exposed crystal facets of Fe_2O_3 has not been revealed. This work disclosed that nanorod-like α-Fe_2O_3 (Fe_2O_3−NR) predominantly exposing (110) facet performed better than nanosheet-like α-Fe_2O_3 (Fe_2O_3−NS) predominantly exposing (001) facet in NH_3−SCR reaction, due to the advantages of Fe_2O_3−NR in redox properties and surface acidity. Furthermore, the results of the SO_2/H_2O resistance test at a critical temperature of 250 °C, catalytic performance evaluations on Fe_2O_3−NR and Fe_2O_3−NS sulfated by $SO_2 + O_2$ or deposited with NH_4HSO_4 (ABS), and systematic characterization revealed that the reactivity of ammonium sulfates on Fe_2O_3 catalysts to NO(+O_2) contributed to their improved catalytic performance, while ferric sulfates showed enhancing and inhibiting effects on NH_3−SCR activity on Fe_2O_3−NR and Fe_2O_3−NS, respectively; despite this, Fe_2O_3−NR showed higher affinity for $SO_2 + O_2$. This work set a milestone in understanding the NH_3−SCR reaction on Fe_2O_3 catalysts in the presence of SO_2 from the aspect of crystal facet engineering.

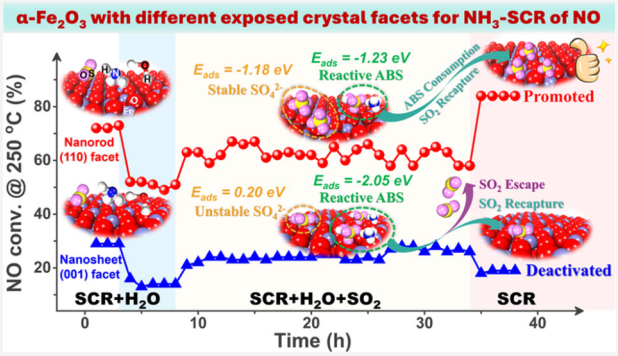

KEYWORDS: *NH_3-SCR of NO_x, α-Fe_2O_3, crystal facet engineering, reaction mechanism, SO_2 resistance, ferric sulfates, ammonium sulfates*

1. INTRODUCTION

In recent decades, significant success has been achieved in NO_x emission control worldwide due to the stringent regulations and efforts from both industry and academia.[1] Among those strategies for NO_x elimination,[2−4] selective catalytic reduction of NO_x by NH_3 (NH_3−SCR of NO_x) is the most widely applied.[5−7] Although the commercial V_2O_5−$WO_3(MoO_3)$/TiO_2 catalyst has been proven to be capable of efficient NH_3−SCR of NO_x in high-temperature (>300 °C) flue gas emitted by electric-power industry, the new requirements for the NO_x emission control in nonelectric industries made V_2O_5−$WO_3(MoO_3)/TiO_2$ sometimes incompetent due to the low temperature of flue gas containing multiple toxic elements (e.g., SO_2, H_2O, alkali and chloride, etc.). Besides, the discarded V_2O_5−$WO_3(MoO_3)/TiO_2$ catalyst is considered a new solid pollutant because of the biological toxicity of vanadium.[8] As a result, an urgent need for environmentally friendly, low-temperature NH_3−SCR catalysts has been raised.

As one of the most abundant metallic elements in the earth's crust, iron (Fe) and its oxides have been extensively applied in the catalysis field due to their nontoxicity, low price, and excellent redox properties.[9−11] In NH_3−SCR reaction, Fe-based catalysts were also reported to exhibit fine catalytic activity and superior resistance to SO_2 poisoning. Similar to the design of various metal oxide catalysts for NH_3−SCR of NO_x, the modulation of the redox property and surface acidity is the most common strategy for increasing the NH_3−SCR activity on Fe-based catalysts. For example, NH_3−SCR activity on Fe_2O_3 catalysts could be promoted via the modification by WO_3 due to the enhanced surface acidity.[12] Fe_2O_3 catalysts doped with CeO_2, CuO, or MnO_x showed excellent low-temperature NH_3−SCR activity because the electronic interactions between Fe and doped metals could significantly boost the redox performance of Fe_2O_3.[13−16] Tuning the morphology or predominantly exposed facets of Fe_2O_3 catalysts could also be used to modulate the redox property and surface acidity, thereby altering the NH_3−SCR perform-

Received: January 8, 2024
Revised: April 15, 2024
Accepted: April 30, 2024
Published: May 8, 2024

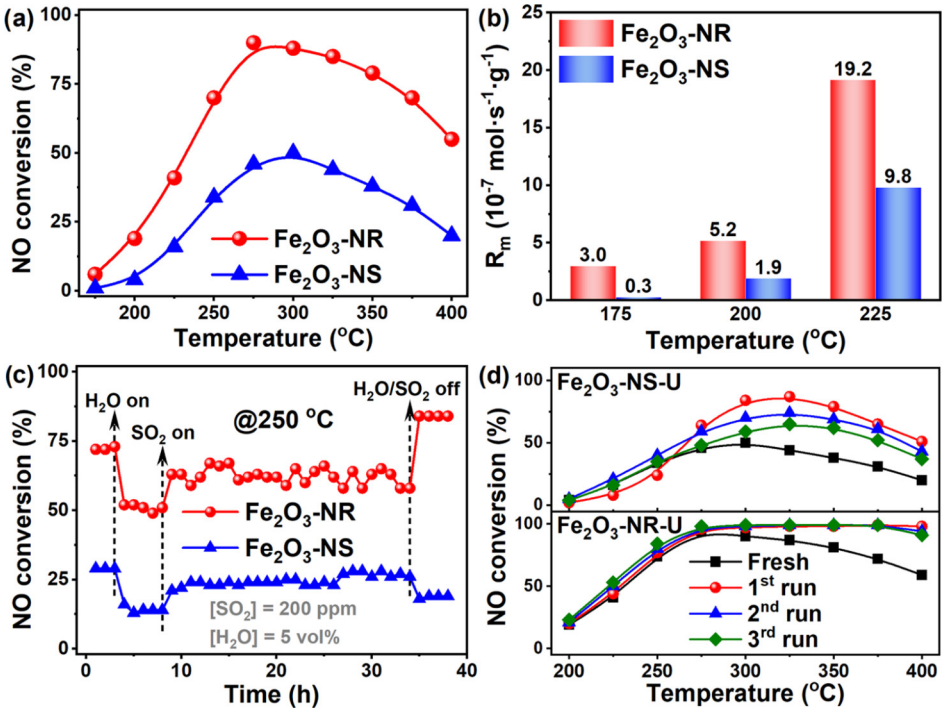

Figure 1. (a) NO conversion on Fe_2O_3 catalysts in NH_3−SCR reaction. Reaction conditions: 500 ppm NO, 500 ppm NH_3, 5 vol % O_2, N_2 as balance. (b) R_m (reaction rates normalized to the mass of catalysts) on Fe_2O_3−NR and Fe_2O_3−NS catalysts in NH_3−SCR reaction. (c) NO conversions on Fe_2O_3−NR and Fe_2O_3−NS catalysts in NH_3−SCR reaction at 250 °C in the presence of SO_2 and H_2O (200 ppm SO_2, 5 vol % H_2O). (d) NH_3−SCR activity on Fe_2O_3−NR-U and Fe_2O_3−NS-U in a three-round cyclic test from 200 to 400 °C. NO conversion on fresh Fe_2O_3−NR and Fe_2O_3−NS were used as references.

ance of Fe_2O_3 catalysts.[17,18] Unlike there is a clear logic used to choose appropriate strategies to improve the NH_3−SCR activity on metal oxide catalysts, it is not easy to conclude a general theory to guide the design of catalysts with excellent resistance to SO_2 poisoning, since various sulfate species (e.g., $(NH_4)_2SO_3$, $(NH_4)_2SO_4$, NH_4HSO_4, metal sulfates, etc.)[19,20] would be formed on catalysts under different reaction conditions after complex surface adsorption and reaction processes. Typically, it has been reported that SO_2 would result in the poisoning of catalysts due to the formation of metal sulfates weakening the redox performance of metal sites and the deposition of NH_4HSO_4 (ABS) covering surface active sites.[20,21] However, it should be noted that some sulfate species are even beneficial to catalysts by serving as acid sites.[22−25] Yu et al. reported that the adsorption of SO_2 would cut off Langmuir−Hinshelwood (L−H) reaction pathway on Fe_2O_3 catalysts by inhibiting the adsorption of NO, thus resulting in the decrease in its NH_3−SCR activity, while ferric sulfates species could act as Brønsted acid sites for NH_3 adsorption and activation and then contribute to the improved NH_3−SCR activity.[26] The deposited ABS on Fe_2O_3 catalysts might also exhibit inhibiting or promotional effects through covering the active sites or reacting with NO + O_2, respectively.[27] In terms of the transformation between different sulfate species (i.e., ferric sulfates and ammonium sulfates), Gu et al. disclosed that SO_4^{2-} in NH_4HSO_4 (ABS) could be trapped by Fe_2O_3 during the decompose/consumption of ABS, and the generated ferric sulfates on Fe_2O_3 could boost the NH_3−SCR activity on Fe_2O_3.[28] However, to the best of our knowledge, the present reported work seldom focused on discussing the impact of different sulfate species on the catalytic performance of Fe_2O_3 catalysts from an aspect of crystal facet engineering, which actually could better guide the design of effective Fe-based NH_3−SCR catalysts with satisfactory SO_2 resistance at the level of microstructure. Inferred from the previous report on the structure−activity relationship on much more intensively discussed CeO_2 catalysts with different morphologies/exposed crystal facets in NH_3−SCR reaction,[19,29,30] it could be proposed that the specific role of different sulfate species in impacting the NH_3−SCR activity on Fe_2O_3 catalysts might also show a morphology/exposed crystal facet dependence.

In this work, starting with the preparation of nanorod-like α-Fe_2O_3 (Fe_2O_3−NR) and nanosheet-like α-Fe_2O_3 (Fe_2O_3−NS) predominantly exposing different crystal facets, the SO_2/H_2O resistance test, and catalytic performance evaluations on Fe_2O_3−NR and Fe_2O_3−NS sulfated by SO_2 + O_2 or deposited with NH_4HSO_4 (ABS) and systematic characterization were conducted to reveal in depth the potential poisoning or promotional effect of different sulfate species on Fe_2O_3 catalysts and their morphology/exposed crystal facet dependence.

2. MATERIALS AND EXPERIMENTAL METHODS

2.1. Catalyst Preparation. α-Fe_2O_3 catalysts in the shape of nanorods (Fe_2O_3−NR) and nanosheets (Fe_2O_3−NS) were prepared by hydrothermal method, as reported elsewhere.[5,31] Detailed preparation processes can be found in Supporting Information (Text S1). Fe_2O_3−NR and Fe_2O_3−NS after the SO_2 + H_2O resistance test were denoted Fe_2O_3−NR-U and Fe_2O_3−NS-U, respectively. Fe_2O_3−NR and Fe_2O_3−NS impregnated with 5 wt % NH_4HSO_4 (ABS) and dried overnight at 110 °C were denoted Fe_2O_3−NR-N or Fe_2O_3−NS-N, respectively. The catalysts (200 mg) sulfated by a flow

https://doi.org/10.1021/acs.est.4c00276
Environ. Sci. Technol. 2024, 58, 8955−8965

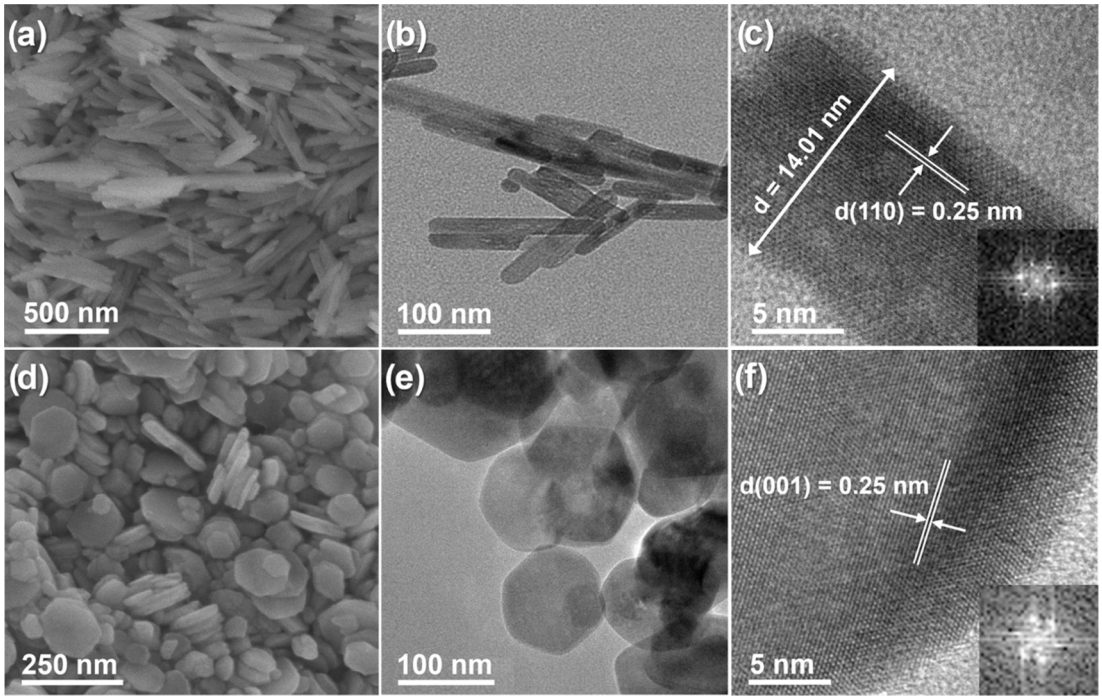

Figure 2. SEM, TEM, and HR-TEM images of (a–c) Fe_2O_3–NR and (d–f) Fe_2O_3–NS.

of 1000 ppm SO_2 + 5 vol % O_2 (total flow rate = 100 mL·min^{-1}) for 1 h were suffixed with "-S".

2.2. Catalyst Characterization and Catalytic Performance Evaluation. The details of catalyst characterization and catalytic performance evaluation can be found in the Supporting Information (Texts S1 and S2).

3. RESULTS AND DISCUSSION

3.1. Catalytic Performance. NO conversion and N_2 selectivity on Fe_2O_3–NR and Fe_2O_3–NS were first measured to estimate their catalytic performance in NH_3–SCR of NO (Figures 1a and S1). Fe_2O_3–NR showed much higher NO conversion and N_2 selectivity than Fe_2O_3–NS. A broad operation temperature window (NO conversion > 80%, N_2 selectivity > 90%) from 275 to 350 °C was achieved on Fe_2O_3–NR, but Fe_2O_3–NS showed much lower NO conversion (< 50%) and N_2 selectivity (< 65%) throughout the entire test temperature range. The generation of abundant N_2O should be the main reason for the poor N_2 selectivity on Fe_2O_3–NS compared to Fe_2O_3–NR (Figure S2). In addition, the decrease in NO conversion and N_2 selectivity at high temperatures (> 375 °C) on Fe_2O_3–NR should be related to the nonselective oxidation of NH_3 to NO and NO_2.[32,33] To further compare the intrinsic activity on Fe_2O_3–NR and Fe_2O_3–NS in NH_3–SCR reaction, kinetic studies were carried out. As shown in Figure 1b and Table S2, the R_m (reaction rates normalized to the mass of catalysts) on Fe_2O_3–NR was 2.0–10.0 times that on Fe_2O_3–NS. Moreover, considering that the specific surface area of Fe_2O_3–NR (18 $m^2 \cdot g^{-1}$) was higher than that of Fe_2O_3–NS (10 $m^2 \cdot g^{-1}$, Table S1), the reaction rate normalized to the specific surface area of catalysts (R_s) was also calculated to see if the specific surface area of Fe_2O_3 catalysts was the main reason for the higher NH_3–SCR activity on Fe_2O_3–NR (Figure S3a). It was found that R_s on Fe_2O_3–NR was still higher than that on Fe_2O_3–NS, confirming that the intrinsic active sites on Fe_2O_3–NR were much more active than those on Fe_2O_3–NS. In addition, the fact that Fe_2O_3–NR (64.8 kJ·mol^{-1}) showed lower apparent activation energy (E_a) than Fe_2O_3–NS (107.3 kJ·mol^{-1}) also indicated that Fe_2O_3–NR could better catalyze the NH_3–SCR of NO (Figure S3b).

Considering that SO_2 and H_2O in exhaust gas emitted by stationary sources or mobile sources would lead to catalyst poisoning, the catalytic performance of Fe_2O_3 catalysts was also evaluated at 250 °C in the presence of 5 vol % H_2O and 200 ppm SO_2 (Figure 1c). After the introduction of H_2O, NO conversion on both Fe_2O_3–NR and Fe_2O_3–NS decreased significantly, which could be due to the competitive adsorption between H_2O and NH_3 or NO_x.[26,33,34] Subsequently, with the introduction of SO_2, NO conversion on Fe_2O_3–NR (ca. 50%) and Fe_2O_3–NS (ca. 10%) increased to ca. 65, and ca. 25%, respectively. After switching off H_2O and SO_2, it was interesting to observe that the NO conversion on Fe_2O_3–NR increased rapidly to ca. 85%, which even surpassed that on fresh Fe_2O_3–NR, indicating that deposited sulfate species were favorable for the NH_3–SCR reaction on Fe_2O_3–NR. As for Fe_2O_3–NS, NO conversion decreased slightly to ca. 20%. To better understand the impact of SO_2 and H_2O on the catalytic performance of Fe_2O_3 catalysts, a cyclic test was conducted on the catalysts used in SO_2/H_2O resistance test (Fe_2O_3–NR-U and Fe_2O_3–NS-U). Fe_2O_3–NR-U was found to show superior stability during the test and performed better than fresh Fe_2O_3–NR (Figure 1d), indicating that sulfur-containing species deposited on Fe_2O_3–NR were beneficial to the proceeding of NH_3–SCR reaction on Fe_2O_3 catalysts. In clear contrast, although Fe_2O_3–NS-U also exhibited higher NH_3–SCR activity than fresh Fe_2O_3–NS at a high temperature range (>275 °C), NO conversion at 275–400 °C on it decreased continuously during the cyclic test, implying that the deposited sulfur-containing species might be converted, decomposed, or consumed during the test, especially at relatively high temperatures (>250 °C). The gradually increasing NH_3–SCR activity on Fe_2O_3–NS-U at a low

https://doi.org/10.1021/acs.est.4c00276
Environ. Sci. Technol. 2024, 58, 8955–8965

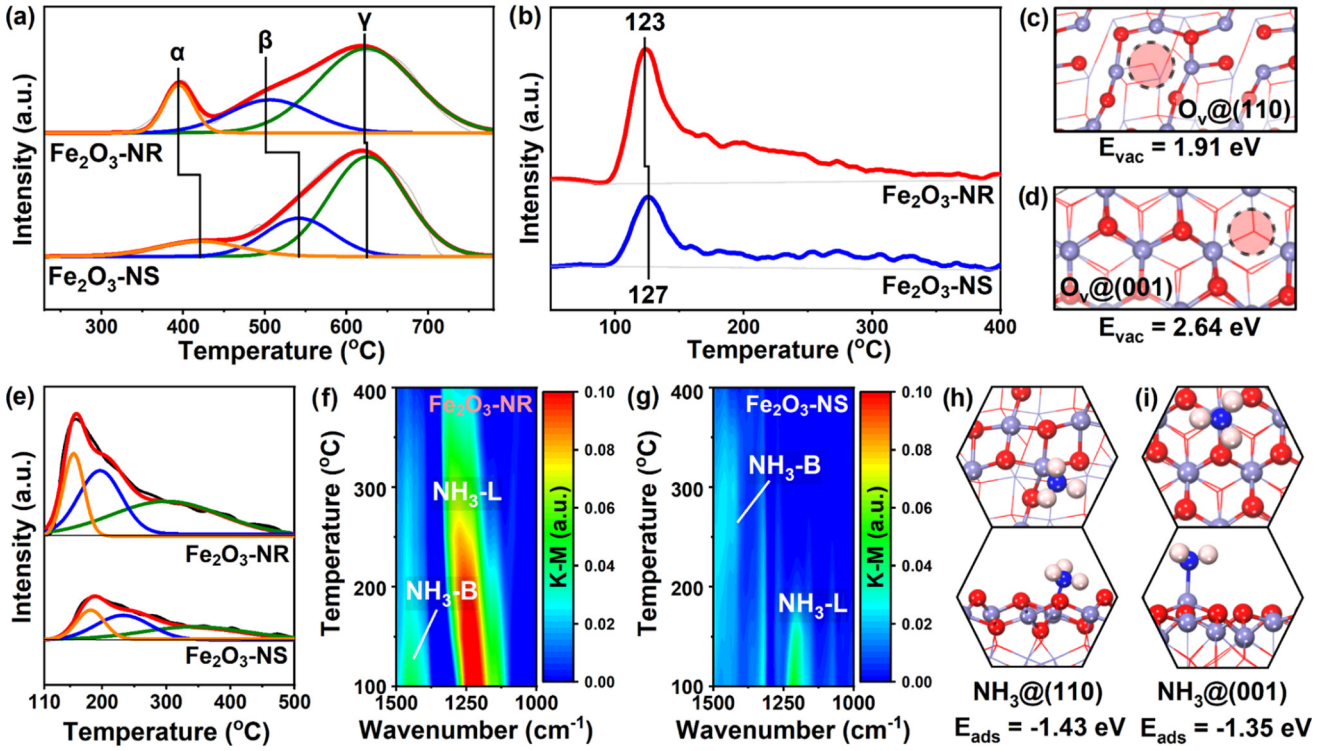

Figure 3. (a) H_2-TPR and (b) O_2-TPD profiles for Fe_2O_3−NR and Fe_2O_3−NS. The optimized surface configuration (with a surface oxygen vacancy) of (c) Fe_2O_3−NR exposing (110) facet and (d) Fe_2O_3−NS exposing (001) facet. (e) NH_3-TPD profiles for Fe_2O_3−NR and Fe_2O_3−NS. *In situ* DRIFTS of NH_3 adsorption on (f) Fe_2O_3−NR and (h) Fe_2O_3−NS. Optimized model of NH_3 adsorption on the Brønsted acid sites on (g) Fe_2O_3−NR and (i) Fe_2O_3−NS.

temperature range (≤250 °C) further confirmed the depletion of sulfate species during the cyclic test. Moreover, the higher NH_3−SCR activity on Fe_2O_3−NR-U suggested that an appropriate sulfation treatment could be used to boost the catalytic performance of Fe_2O_3−NR.

3.2. Structural Information. To determine the crystal phase of the prepared Fe_2O_3 catalysts, their XRD patterns were collected (Figure S4). All diffraction peaks on Fe_2O_3−NR and Fe_2O_3−NS could be indexed to pure α-Fe_2O_3 (Hematite #87−1164). Scanning electron microscopy (SEM), transmission electron microscopy (TEM), and High-resolution-TEM (HR-TEM) images of Fe_2O_3 catalysts were also collected and shown in Figure 2. Fe_2O_3−NR was in a nanorod shape with a length of 150−500 nm and a diameter of 15−30 nm. The clear interplanar distance of 0.25 nm on Fe_2O_3−NR matched well with the d_{110} spacing of pure hexagonal hematite.[13,35] Fe_2O_3−NS was in a regular ortho-hexagonal nanosheet shape with well-defined edges. The diameter and the thickness of ortho-hexagonal NSs were 50−150 and 10−30 nm, respectively. In addition, the lattice spacing of 0.25 nm in the HR-TEM image of Fe_2O_3−NS (Figure 2f) was related to the $(11\bar{2}0)$ plane and the inserted FFT pattern showed six equivalent 1120 points, indicating that the top and bottom surfaces of the horizontally placed nanocrystals belong to the (0001) and $(000\bar{1})$ planes, respectively.[35] In short, Fe_2O_3 NR exposing (110) crystal facet and Fe_2O_3 NS exposing (001) crystal facet were successfully prepared.

3.3. Redox and Surface Acidity. Since the NH_3−SCR reaction was composed of two half-reaction cycles, i.e., redox cycle and acid cycle, systematic characterization was conducted to evaluate the redox property and surface acidity of Fe_2O_3 catalysts. As shown in Figure 3a and Table S3, three H_2-consumption peaks were observed on both Fe_2O_3−NR and Fe_2O_3−NS from a low temperature to a high temperature (α, β, and γ), which could be attributed to the reduction of Fe_2O_3 to Fe_3O_4, Fe_3O_4 to FeO, and FeO to Fe, respectively.[36,37] The reduction of Fe_2O_3−NR at lower temperatures suggested that Fe_2O_3−NR showed better redox performance, which could be further supported by the results of O_2-TPD that more active chemisorbed oxygen species were formed on Fe_2O_3−NR (Figure 3b and Table S4). The higher concentration of surface Fe^{2+} species and adsorbed oxygen species on Fe_2O_3−NR indicated that Fe_2O_3−NR could better activate oxygen species (Figure S5).[26,38] Based on the optimized surface configuration of Fe_2O_3−NR exposing (110) facet and Fe_2O_3−NS exposing (001) facet, the oxygen defect formation energy (E_{vac}) was also determined by theoretical calculations (Figure 3c,d). The much lower E_{vac} on Fe_2O_3−NR (1.91 eV) than that on Fe_2O_3−NS (2.64 eV) further confirmed that oxygen defects could be more easily formed on Fe_2O_3−NR, thus facilitating the adsorption/activation of oxygen species and resulting in better redox performance.

NH_3-TPD experiments were conducted to investigate the surface acidity of Fe_2O_3 catalysts (Figure 3e and Table S5).[26] Fe_2O_3−NR possessed much more acid sites than Fe_2O_3−NS, even in terms of specific surface area per unit. To further determine the type of surface acid sites and investigate their acid strength, *in situ* DRIFTS of NH_3-TPD experiments were performed (Figure 3f,g). The intensive band at ca. 1220 cm^{-1} could be attributed to NH_3 adsorbed on Fe^{3+} sites serving as Lewis acid sites (NH_3−L),[39] while the relatively weaker band at ca. 1450 cm^{-1} was related to NH_3 species adsorbed on

https://doi.org/10.1021/acs.est.4c00276
Environ. Sci. Technol. 2024, 58, 8955−8965

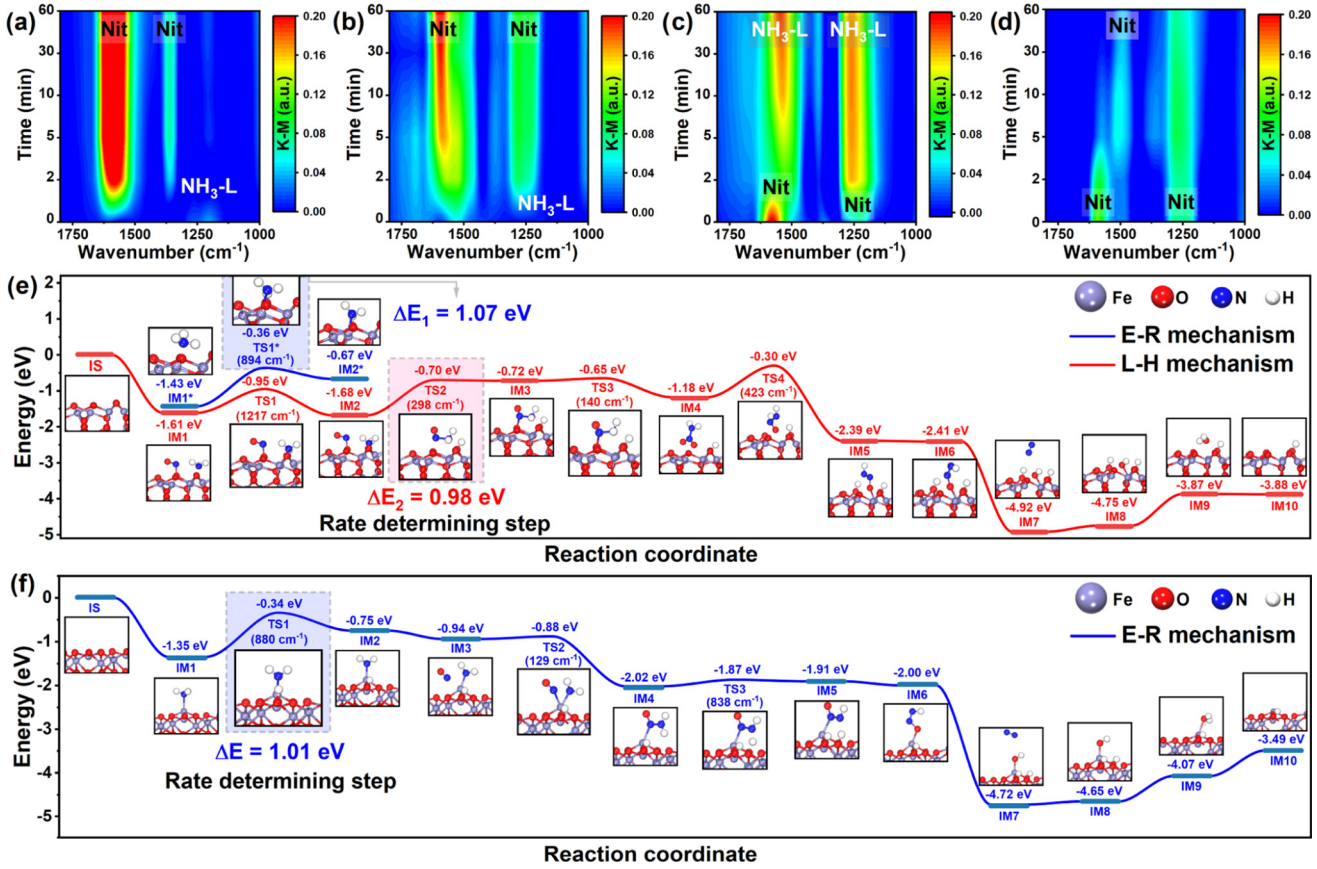

Figure 4. *In situ* DRIFTS of NO+O_2 reacting with adsorbed NH_3 on (a) Fe_2O_3−NR and (b) Fe_2O_3−NS. *In situ* DRIFTS of NH_3 reacting with adsorbed NO + O_2 on (c) Fe_2O_3−NR and (d) Fe_2O_3−NS catalysts. All of the spectra were collected at 200 °C. Reaction conditions: 500 ppm NO (when used), 500 ppm NH_3 (when used), 5 vol % O_2 (when used), and N_2 as balance (Total flow rate = 50 mL·min^{-1}). (e) Proposed detailed reaction pathway of NH_3−SCR reaction on Fe_2O_3−NR followed E−R or L−H mechanism. (f) Proposed detailed reaction pathway of NH_3−SCR reaction on Fe_2O_3−NS, followed E−R mechanism. Purple, red, blue, and white balls represented Fe, O, N, and H atoms, respectively. The imaginary frequency of all transition states was calculated and attached in parentheses.

Brønsted acid sites (NH_3−B),[13] indicating that acid sites on Fe_2O_3−NR and Fe_2O_3−NS were mainly in the form of Lewis acid sites. Furthermore, NH_3−L species on Fe_2O_3−NR would desorb at higher temperatures than those on Fe_2O_3−NS. That is, Lewis acid sites on Fe_2O_3−NR showed higher acid strength (Figure 3h,i), which was further supported by the theoretical calculation on NH_3 adsorption energy (E_{ads}) that Fe_2O_3−NR (E_{ads} = −1.43 eV) exhibited higher E_{ads} than Fe_2O_3−NS (E_{ads} = −1.35 eV). In short summary, the better redox performance and more surface acid sites should be the main reasons for the higher NH_3−SCR activity on Fe_2O_3−NR compared to Fe_2O_3−NS.

3.4. Reaction Mechanism. To investigate the reaction mechanism on the prepared Fe_2O_3 catalysts, *in situ* DRIFTS experiments of NO + O_2 reacting with preadsorbed NH_3 and NH_3 reacting with preadsorbed NO_x were performed at 200 °C. As shown in Figures 4a,b and S6a,b, the barely observable NH_3−B species on both Fe_2O_3−NR and Fe_2O_3−NS at 200 °C hinted that Brønsted acid sites with relatively weaker acid strength were not the main reactive species. For both Fe_2O_3−NR and Fe_2O_3−NS, NH_3−L species could be consumed by NO + O_2 rapidly, indicating that NH_3−SCR reaction on these two Fe_2O_3 catalysts could be proceeded efficiently by Eley−Rideal (E−R) mechanism. More Lewis acid sites on Fe_2O_3−NR enabled its higher NH_3−SCR activity. The reactivity of preadsorbed NO_x species to NH_3 was further explored to see if the NH_3−SCR reaction on Fe_2O_3−NR and Fe_2O_3−NS could also be proceeded by Langmuir−Hinshelwood (L−H) mechanism. As illustrated in Figures 4c and S6c, the nitrate species on Fe_2O_3−NR were dominantly in the form of bridged nitrates (1224 and 1596 cm^{-1}),[13] which could readily react with NH_3, indicating that the NH_3−SCR reaction on Fe_2O_3−NR could also follow L−H mechanism. Differently, bridged nitrate species (1596 cm^{-1})[13] and monodentate nitrates (1480 and 1293 cm^{-1})[40] on Fe_2O_3−NS showed much lower reactivity to NH_3 (Figures 4d and S6d), which meant that L−H mechanism was not the dominant reaction mechanism on Fe_2O_3−NS. According to the results of DRIFTS study, it could be proposed that NH_3−SCR reaction on Fe_2O_3−NS was mainly proceeded by E−R mechanism, while for Fe_2O_3−NR, NH_3−SCR reaction on it seemed to follow both E−R and L−H mechanisms.

Theoretical calculations were conducted to further determine the dominant reaction pathway on Fe_2O_3−NR (Figures 4e and S7a). For L−H mechanism on Fe_2O_3−NR, the step of N−N coupling (IM2 → TS2) required the highest energy (0.98 eV) to overcome the energy barrier, indicating that N−N coupling was the rate-determining step for NH_3−SCR reaction following L−H mechanism on Fe_2O_3−NR. In E−R mechanism, since the NH_3 activation is always the rate-determining

https://doi.org/10.1021/acs.est.4c00276
Environ. Sci. Technol. 2024, 58, 8955−8965

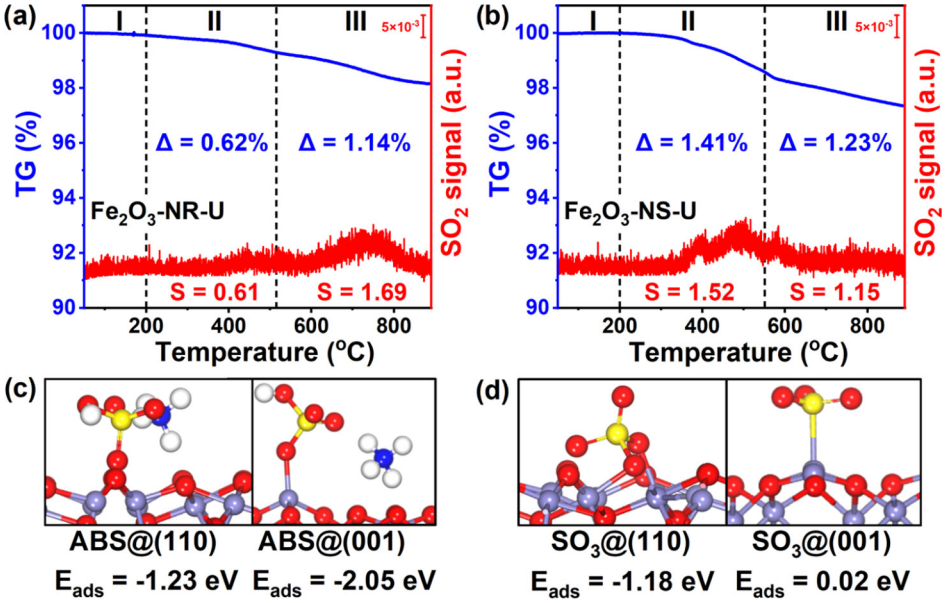

Figure 5. TG-MS curves of (a) Fe_2O_3−NR-U and (b) Fe_2O_3−NS-U. The adsorption energy of (c) ABS and (d) SO_3 on Fe_2O_3−NR exposing (110) facet and Fe_2O_3−NS exposing (001) facet.

step,[41] the energy barrier of NH_3 activation on Fe_2O_3−NR was also calculated. The energy barrier of NH_3 activation (IM1* → TS1*, 1.07 eV) was found to be higher than the energy barrier of the N−N coupling step (0.98 eV), suggesting that Fe_2O_3−NR could better catalyze NH_3−SCR reaction through L−H mechanism (Figures 4e and S7b). The rate-determining step of NH_3−SCR reaction following E−R mechanism on Fe_2O_3−NS was also investigated (Figures 4f and S8). It was revealed that the activation of NH_3 (IM1* → TS1*) was the rate-determining step with an energy barrier of 1.01 eV, slightly higher than the energy barrier of the rate-determining step of NH_3−SCR reaction following L−H mechanism on Fe_2O_3−NR (0.98 eV), further explaining why Fe_2O_3−NR exhibited higher NH_3−SCR activity than Fe_2O_3−NS. Since it has been confirmed that the NH_3−SCR reaction on Fe_2O_3−NS mainly followed E−R mechanism, L−H pathway on Fe_2O_3−NS was not considered in theoretical calculation.

3.5. Impact of SO_2 and H_2O on the NH_3−SCR Performance of Fe_2O_3 Catalysts. SO_2 and H_2O in the flue gas would result in the poisoning of NH_3−SCR catalysts, which made the investigation of the SO_2/H_2O poisoning effect and the development of efficient NH_3−SCR catalysts with superior SO_2/H_2O resistance become research hotspots. As shown in Figure 1c, although both Fe_2O_3−NR and Fe_2O_3−NS suffered from varying degrees of deactivation in the presence of SO_2 and H_2O, NO conversion on Fe_2O_3−NR increased rapidly after switching off SO_2 and H_2O, which was even higher than that on fresh Fe_2O_3−NR. So, the deposited sulfate species might show a promotion or inhibition effect on Fe_2O_3 catalysts under different reaction conditions. The absence of XRD peaks related to crystalline sulfated Fe species (e.g., $Fe_2(SO_3)_3$, $Fe_2(SO_4)_3$, $FeOSO_4$, etc.) on the XRD patterns for both Fe_2O_3−NR-U and Fe_2O_3−NS-U indicated that the sulfate species on used catalysts were mainly in the form of amorphous surface ferric sulfates or ammonium sulfates (Figure S4).[26] The specific surface area of the used catalysts showed no limited decrease compared to fresh catalysts (Table S1), confirming that the decrease/increase in the NO conversion on Fe_2O_3 catalysts in SO_2 + H_2O resistance test was not due to the change in the crystal structure.

To further determine the amount of sulfate species on used Fe_2O_3 catalysts and identify their types, thermogravimetric and mass spectrometric (TG-MS) analysis was conducted on Fe_2O_3−NR-U and Fe_2O_3−NS-U. Just as reported by Zhang and Song et al., TG curves for NH_3−SCR catalysts used in NH_3−SCR reaction could always be divided into three steps (i.e., 25−200, 200−550, and 550−800 °C), which could be related to the desorption or decomposition of H_2O, NH_4HSO_4, and metal sulfates, respectively,[2,42] and there were three weight loss steps in TG-MS profiles for Fe_2O_3−NR-U and Fe_2O_3−NS-U from low to high temperatures (Figure 5a,b). Step I (room temperature → 200 °C) and step II (200, → 550 °C) could be related to the desorption of adsorbed H_2O and the decomposition of ammonium sulfates, respectively. Step III could be attributed to the decomposition of ferric sulfates and possible O_2 desorption. As shown in Figure 5a and Table S6, the weight loss value of step II on Fe_2O_3−NR-U (0.62%) was lower than that on Fe_2O_3−NS-U (1.41%), indicating the formation of more ammonium sulfates on Fe_2O_3−NS-U. The observation of two SO_2 desorption peaks within step II suggested that the ammonium sulfate species on Fe_2O_3−NS-U could be classified into two types, i.e., ammonium sulfates in loose contact with the catalysts and ammonium sulfates in close contact with the catalysts. The weight loss value of step III on Fe_2O_3−NR-U (1.14%) was still lower than that on Fe_2O_3−NS-U (1.23%). However, according to the MS signals of SO_2, it could be asserted that step III on Fe_2O_3−NS-U was mainly related to O_2 desorption instead of sulfate decomposition (Figure 5b). Considering that SO_2 released from the decomposition of ammonium sulfates might be recaptured by Fe_2O_3 below 550 °C,[43] the much more intensive SO_2 signal in step III on Fe_2O_3−NR-U and the faint SO_2 signal in step III on Fe_2O_3−NS-U suggested that SO_2 could easier react with Fe_2O_3−NR compared to Fe_2O_3−NS. To further explore the affinity of Fe_2O_3 catalysts for different sulfate species, the adsorption energy (E_{ads}) of ammonium

https://doi.org/10.1021/acs.est.4c00276
Environ. Sci. Technol. 2024, 58, 8955−8965

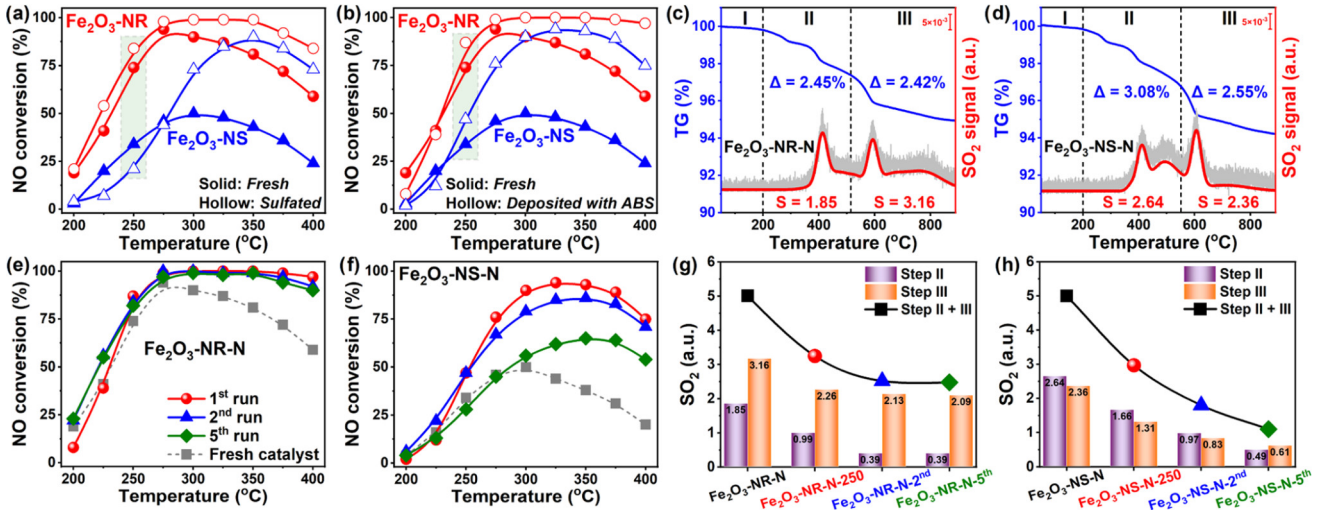

Figure 6. (a) NH_3−SCR activity on Fe_2O_3−NR, Fe_2O_3−NS, Fe_2O_3−NR-S, and Fe_2O_3−NS-S ("−S" meant sulfation treatment by $SO_2 + O_2$). (b) NH_3−SCR activity on Fe_2O_3−NR, Fe_2O_3−NS, Fe_2O_3−NR-N, and Fe_2O_3−NS-N ("−N" meant catalyst deposited with ABS). TG-MS plots for (c) Fe_2O_3−NR-N and (d) Fe_2O_3−NS-N. NH_3−SCR activity on (e) Fe_2O_3−NR-N and (f) Fe_2O_3−NS-N in the cyclic test. The relative amount of SO_2 desorbed from (g) Fe_2O_3−NR-N, Fe_2O_3−NR-N-250, Fe_2O_3−NR-N-2nd, and Fe_2O_3−NR-N-5th and (h) Fe_2O_3−NS-N, Fe_2O_3−NS-N-250, Fe_2O_3−NS-N-2nd, and Fe_2O_3−NS-N-5th calculated based on the SO_2 plots in TG-MS experiments.

sulfates (using NH_4HSO_4 (ABS) as an example) and SO_3 on Fe_2O_3−NR exposing (110) facet and Fe_2O_3−NS exposing (001) facet was calculated theoretically (Figure 5c,d).[26,44] It was disclosed that E_{ads} of ABS (−1.23 eV) was lower than E_{ads} of SO_3 (−2.05 eV) on Fe_2O_3−NR exposing (110) facet, while E_{ads} of ABS (−1.18 eV) was higher than E_{ads} of SO_3 (0.02 eV) on Fe_2O_3−NS exposing (110) facet, suggesting that the dominant sulfate species on Fe_2O_3−NR and Fe_2O_3−NS were ferric sulfates and ammonium sulfates, respectively.

To better disclose the effect of ferric sulfates and ammonium sulfates on the NH_3−SCR activity on Fe_2O_3−NR and Fe_2O_3−NS, NO conversions on Fe_2O_3 catalysts sulfated with $SO_2 + O_2$ flow (suffixed with "-S") and impregnated with ABS (suffixed with "-N") were measured. As shown in Figure 6a, Fe_2O_3−NR-S showed better activity than fresh Fe_2O_3−NR throughout the testing temperature range from 200 to 400 °C. Differently, although the ferric sulfates on Fe_2O_3−NS were found to facilitate the proceeding of NH_3−SCR reaction at high temperatures (>275 °C), they resulted in the deactivation of Fe_2O_3−NS when the temperature was lower than 275 °C. That is, surface ferric sulfates showed promotion and inhibition effects on the catalytic activity of Fe_2O_3−NR and Fe_2O_3−NS at 250 °C, respectively. However, N_2 selectivity on both Fe_2O_3−NR and Fe_2O_3−NS was improved after sulfation treatment (Figure S9a), which should be due to the suppression of nonselective oxidation of NH_3.[45] TG-MS experiments on sulfated Fe_2O_3 catalysts showed that more SO_2 was adsorbed on Fe_2O_3−NR than on Fe_2O_3−NS under the same sulfation condition (Figure S10 and Table S6), well supporting the results of theoretical calculations that SO_3 were easily adsorbed on Fe_2O_3−NR compared to Fe_2O_3−NS. As reported previously, the sulfation of metal oxides (e.g., CeO_2, Fe_2O_3, PrO_x, etc.) might lead to the increase in its NH_3−SCR activity because metal sulfates could serve as acid sites for NH_3 adsorption and activation even though the formation of metal sulfates always weakened the low-temperature redox capability of metal oxides.[20,24,27,45−47] In this work, the enhancement in the surface acidity of Fe_2O_3−NR and Fe_2O_3−NS after the sulfation treatment as suggested by the results of NH_3-TPD (Figure S11 and Table S5) should be the main reason for their improved NH_3−SCR activity, especially at high temperatures (>275 °C), while the formation of ferric sulfates on Fe_2O_3−NS still resulted in the deactivation at low temperatures (<275 °C). Besides, it was revealed by *in situ* DRIFTS study that NH_3−SCR reaction on Fe_2O_3−NR and Fe_2O_3−NS was proceeded by E−R mechanism due to the enhanced surface acidity and significantly inhibited NO_x adsorption (Figure S12).

As for Fe_2O_3 catalysts impregnated with ABS (Figures 6b and S9b), improved NH_3−SCR activity and N_2 selectivity were achieved on both Fe_2O_3−NR-N and Fe_2O_3−NS-N when the reaction temperature reached 250 °C or higher. Moreover, although the deposition of ammonium sulfates has been widely recognized to result in the deactivation of NH_3−SCR catalysts because of the coverage of active sites by it, it was also reported that NH_4^+ of ABS could react with gaseous NO_2.[26,37,48−50] TG-MS experiments were then carried out on Fe_2O_3−NR-N and Fe_2O_3−NS-N to investigate the thermal stability of ABS on different Fe_2O_3 catalysts. As shown in Figure 6c,d, although Fe_2O_3−NR-N and Fe_2O_3−NS-N showed an identical total amount of desorbed SO_2 throughout the heating process, it was noticeable that a higher amount of SO_2 was desorbed from Fe_2O_3−NR-N (3.16) than Fe_2O_3−NS-N (2.36) during step III, confirming that SO_2 released from ABS decomposition was much easier to be recaptured by Fe_2O_3−NR.

To further determine the role of ABS in inhibiting or promoting the catalytic performance of Fe_2O_3 catalysts, cyclic NH_3−SCR activity tests were performed (Figures 6e,f and S13). For Fe_2O_3−NR-N, the NO conversion on it showed no change after the 2nd run, and almost the same as that on Fe_2O_3−NR-S, which meant that ABS might decompose during the first two-round test and SO_2 released from ABS would be captured by Fe_2O_3−NR to form surface ferric sulfates, and those ferric sulfates were stable during the test without further escape. On the contrary, Fe_2O_3−NS-N suffered from continuous deactivation during the cyclic test, suggesting that the deposited ABS, which could boost the NH_3−SCR activity on Fe_2O_3−NS, was consumed with significant SO_2 escape,

https://doi.org/10.1021/acs.est.4c00276
Environ. Sci. Technol. 2024, 58, 8955−8965

since Fe_2O_3−NS showed limited reactivity to SO_2 + O_2 compared to Fe_2O_3−NR, as proved by the results of TG-MS experiments on Fe_2O_3−NS-S (Figure S10 and Table S6) and theoretical calculation (Figure 5d).

Aiming at investigating the consumption of ABS during the cyclic tests, TG-MS experiments were also conducted on Fe_2O_3−NR-N and Fe_2O_3−NS-N after the first run to 250 °C, the second run, and the fifth run, which were suffixed with "-N-250", "−2nd", and "−5th", respectively (Figure S14). The amount of SO_2 desorbed from these catalysts was summarized and listed in Figure 6g,h and Table S6. For both Fe_2O_3−NR-N-250 and Fe_2O_3−NS-N-250, the total amount of SO_2 desorbed from them (ca. 5.00) was much less than that desorbed from Fe_2O_3−NR-N (3.25) and Fe_2O_3−NS-N (2.97). Considering that ABS on Fe_2O_3 catalysts would not thermally decompose at 250 °C (Figure 6c,d), it could be proposed that NH_4^+ species in ABS on both Fe_2O_3−NR and Fe_2O_3−NS can react with NO + O_2 at 250 °C. Moreover, it was interesting to observe that the total amount of sulfate species on Fe_2O_3−NR-N remained almost unchanged after the second run, and the SO_2 mainly desorbed in step III in TG-MS experiments (Figure 6g), suggesting that the sulfate species in ABS on Fe_2O_3−NR-N would be converted to stable ferric sulfates due to the consumption of ABS and the recapture of SO_2 by Fe_2O_3−NR. That is why Fe_2O_3−NR-N showed stable and high NO conversions in the cyclic test, and Fe_2O_3−NR-5th showed comparable NO conversion to that on Fe_2O_3−NR-S (Figure S15). As for Fe_2O_3−NS-N, in clear contrast, the continuous decrease in the total amount of surface sulfates in NH_3−SCR reaction flow below 400 °C suggested that the reactants (i.e., NH_3 and NO) could induce the decomposition of SO_4^{2-} (Figure 6h). Considering that NO could hardly strongly interact with SO_4^{2-}, the formation of ammonium sulfate-like species might account for the further weakened interaction between SO_4^{2-} and Fe_2O_3−NS, which resulted in the continuous SO_2 escape under low temperatures (≤400 °C).

Based on the results of systematical characterization, theoretical calculations, and catalytic performance evaluation, the impact of H_2O and SO_2 on the catalytic performance of Fe_2O_3 catalysts could be revealed. After the introduction of H_2O, the competition adsorption between H_2O and NH_3/NO + O_2 would lead to a sharp decrease in NO conversion.[51−54] When SO_2 was also introduced to the feeding gas without cutting off H_2O, a slight increase in NO conversions was observed on both Fe_2O_3−NR and Fe_2O_3−NS due to the formation of surface ferric sulfates and ammonium sulfates, which could serve as acid sites for NH_3 adsorption. After switching off H_2O and SO_2, the competition adsorption between H_2O and NH_3/NO_x that no longer existed contributed to the sharp increase in the NO conversion, and the stable surface ferric sulfates serving as Brønsted acid sites could help further enhance the catalytic performance of Fe_2O_3−NR. However, although the ammonium species generated on Fe_2O_3−NS in the presence of H_2O and SO_2 were highly reactive to NO_x, when H_2O and SO_2 were turned off, the consumption of reactive ABS and the remaining surface ferric sulfates with a poisoning effect at a relatively low temperature range (<275 °C) still resulted in the slight decrease in its NO conversion on Fe_2O_3−NS. To better demonstrate the role of various sulfate species in influencing the catalytic performance of nanoshaped Fe_2O_3 catalysts, a scheme was proposed (Scheme 1). Although both ferric sulfates and ammonium sulfates could help boost the NH_3−SCR activity on Fe_2O_3−NR and Fe_2O_3−NS at a high temperature range (H-*T*, >275 °C), Fe_2O_3−NS would suffer from severe deactivation due to the formation of ferric sulfates at low temperatures (L-*T*, <275 °C).

Scheme 1. Effects of Various Sulfate Species on the Catalytic Performance of Nanoshaped Fe_2O_3 Catalysts Predominantly Exposing Different Facets at Different Temperature Ranges

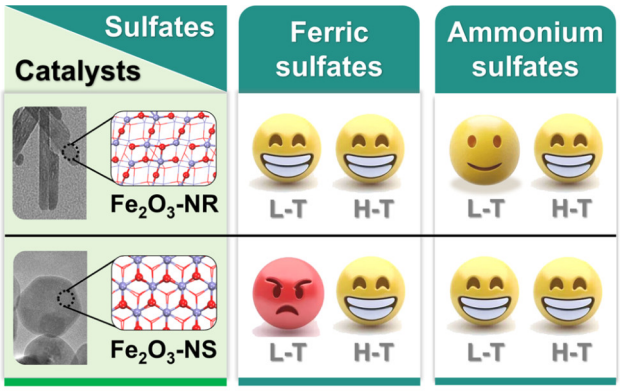

L-T = Low temperature (< 275 °C); H-T = High temperature (> 275 °C)

4. ENVIRONMENTAL IMPLICATIONS

As a widely investigated technology for NO_x removal, satisfactory deNO_x efficiency under an ideal reaction condition without poisoning elements (e.g., SO_2, H_2O, alkali, chlorine, etc.) could be easily achieved over the full temperature range (100−600 °C). However, the purification of flue gas containing high concentrations of SO_2 and H_2O, the most common poisoning molecules, at 250 °C or lower is still a challenge for environment catalysis community. In this work, based on the previous report that Fe_2O_3-based catalysts might be a promising candidate for the NH_3−SCR of NO_x at 250−350 °C with superior SO_2/H_2O resistance, it was further revealed that ammonium sulfates deposited on Fe_2O_3 catalysts were reactive to NO at 250 °C or higher, while the formation of ferric sulfates could be poisoning or promotional to Fe_2O_3 catalysts depending on the predominantly exposed crystal facets. This work is the first to systematically discuss the role of different sulfate species in NH_3−SCR reaction on Fe_2O_3 catalysts from a crystal facet engineering perspective, which provided insights into the development of effective catalysts with superior SO_2/H_2O resistance and thus benefited the whole environment catalysis community.

■ ASSOCIATED CONTENT

Supporting Information

The Supporting Information is available free of charge at https://pubs.acs.org/doi/10.1021/acs.est.4c00276.

Details of catalyst characterization and catalytic performance evaluation; description of the DFT calculation method; product distribution in NH_3−SCR reaction; N_2 selectivity; kinetic study; XRD; XPS; *in situ* DRIFTS of NH_3−SCR reaction; configuration of intermediates and transition states of reactants; TG-MS; NH_3−SCR activity in the cyclic test; N_2 physisorption; H_2-TPR; O_2-TPD; and NH_3-TPD (PDF)

https://doi.org/10.1021/acs.est.4c00276
Environ. Sci. Technol. 2024, 58, 8955−8965

AUTHOR INFORMATION

Corresponding Authors

Wei Tan − *State Key Laboratory of Pollution Control and Resource Reuse, School of Environment, Jiangsu Key Laboratory of Vehicle Emissions Control, Center of Modern Analysis, Key Laboratory of Mesoscopic Chemistry of MOE School of Chemistry and Chemical Engineering, Nanjing University, Nanjing 210023, P. R. China;* orcid.org/0000-0002-1481-9346; Email: tanwei@nju.edu.cn

Chuanzhi Sun − *College of Chemistry, Chemical Engineering and Materials Science, Shandong Provincial Key Laboratory of Clean Production of Fine Chemicals, Institute of Materials and Clean Energy, Shandong Normal University, Jinan 250014, P. R. China;* orcid.org/0000-0002-3744-9800; Email: suncz@sdnu.edu.cn

Authors

Siqing Cheng − *College of Chemistry, Chemical Engineering and Materials Science, Shandong Provincial Key Laboratory of Clean Production of Fine Chemicals, Institute of Materials and Clean Energy, Shandong Normal University, Jinan 250014, P. R. China*

Fang Xu − *College of Chemistry, Chemical Engineering and Materials Science, Shandong Provincial Key Laboratory of Clean Production of Fine Chemicals, Institute of Materials and Clean Energy, Shandong Normal University, Jinan 250014, P. R. China*

Shan Yang − *College of Chemistry, Chemical Engineering and Materials Science, Shandong Provincial Key Laboratory of Clean Production of Fine Chemicals, Institute of Materials and Clean Energy, Shandong Normal University, Jinan 250014, P. R. China*

Bifeng Zhang − *State Key Laboratory of Pollution Control and Resource Reuse, School of Environment, Jiangsu Key Laboratory of Vehicle Emissions Control, Center of Modern Analysis, Key Laboratory of Mesoscopic Chemistry of MOE School of Chemistry and Chemical Engineering, Nanjing University, Nanjing 210023, P. R. China*

Wang Song − *State Key Laboratory of Pollution Control and Resource Reuse, School of Environment, Jiangsu Key Laboratory of Vehicle Emissions Control, Center of Modern Analysis, Key Laboratory of Mesoscopic Chemistry of MOE School of Chemistry and Chemical Engineering, Nanjing University, Nanjing 210023, P. R. China*

Xuechen Zhu − *College of Chemistry, Chemical Engineering and Materials Science, Shandong Provincial Key Laboratory of Clean Production of Fine Chemicals, Institute of Materials and Clean Energy, Shandong Normal University, Jinan 250014, P. R. China*

Lin Dong − *State Key Laboratory of Pollution Control and Resource Reuse, School of Environment, Jiangsu Key Laboratory of Vehicle Emissions Control, Center of Modern Analysis, Key Laboratory of Mesoscopic Chemistry of MOE School of Chemistry and Chemical Engineering, Nanjing University, Nanjing 210023, P. R. China;* orcid.org/0000-0002-8393-6669

Complete contact information is available at: https://pubs.acs.org/10.1021/acs.est.4c00276

Author Contributions

[§]S.C. and F.X. contributed equally to this work.

Notes

The authors declare no competing financial interest.

ACKNOWLEDGMENTS

This work was supported by the National Natural Science Foundation of China (22372093, 21976111, and 22306090), the Shandong Provincial Natural Science Foundation (ZR2019MB052), and the Natural Science Foundation of Jiangsu Province (BK20230773 and BK20231513).

REFERENCES

(1) He, Y.; Tan, Y.; Song, M.; Tu, Q.; Fu, M.; Long, L.; Wu, J.; Xu, M.; Liu, X. Switching on photocatalytic NO oxidation and proton reduction of NH_2-MIL-125 (Ti) by convenient linker defect engineering. *J. Hazard. Mater.* **2022**, *430*, No. 128468.

(2) Zhang, L.; Li, L.; Cao, Y.; Yao, X.; Ge, C.; Gao, F.; Deng, Y.; Tang, C.; Dong, L. Getting insight into the influence of SO_2 on TiO_2/CeO_2 for the selective catalytic reduction of NO by NH_3. *Appl. Catal., B* **2015**, *165*, 589−598.

(3) Castoldi, L.; Matarrese, R.; Morandi, S.; Righini, L.; Lietti, L. New insights on the adsorption, thermal decomposition and reduction of NO_x over Pt-and Ba-based catalysts. *Appl. Catal., B* **2018**, *224*, 249−263.

(4) Wang, D.; Chen, Q.; Zhang, X.; Gao, C.; Wang, B.; Huang, X.; Peng, Y.; Li, J.; Lu, C.; Crittenden, J. Multipollutant control (MPC) of flue gas from stationary sources using SCR technology: a critical review. *Environ. Sci. Technol.* **2021**, *55* (5), 2743−2766.

(5) Qu, W.; Liu, X.; Chen, J.; Dong, Y.; Tang, X.; Chen, Y. Single-atom catalysts reveal the dinuclear characteristic of active sites in NO selective reduction with NH_3. *Nat. Commun.* **2020**, *11* (1), No. 1532.

(6) Liu, J.; He, G.; Shan, W.; Yu, Y.; Huo, Y.; Zhang, Y.; Wang, M.; Yu, R.; Liu, S.; He, H. Introducing tin to develop ternary metal oxides with excellent hydrothermal stability for NH_3 selective catalytic reduction of NO. *Appl. Catal., B* **2021**, *291*, No. 120125.

(7) Huang, Y.; Liu, S.; Pei, M.-M.; Li, J.-Y.; Xu, H.-D.; Chen, Y.-Q. Unveiling H_2O_2-optimized NO_x adsorption-selective catalytic reduction (AdSCR) performance of WO_3/$CeZrO_2$ catalyst. *Rare Met.* **2023**, *42* (11), 3755−3765.

(8) Jin, Q.; Shen, Y.; Cai, Y.; Chu, L.; Zeng, Y. Resource utilization of waste V_2O_5-based deNO_x catalysts for hydrogen production from formaldehyde and water via steam reforming. *J. Hazard. Mater.* **2020**, *381*, No. 120934.

(9) Busca, G.; Lietti, L.; Ramis, G.; Berti, F. Chemical and mechanistic aspects of the selective catalytic reduction of NO_x by ammonia over oxide catalysts: a review. *Appl. Catal., B* **1998**, *18* (1−2), 1−36.

(10) Huang, T.; Zhang, Y.; Zhuang, K.; Zhu, Y.; Kai, S. Preparation of honeycombed holmium-modified Fe-Mn/TiO_2 catalyst and its performance in the low temperature selective catalytic reduction of NO_x. *J. Fuel Chem. Technol.* **2018**, *46* (3), 319−327, DOI: 10.1016/S1872-5813(18)30015-X.

(11) Yang, H.-H.; Qian, X.; Zhang, N.; Jia, X.; Wen, Z.; Chen, X.; Zhou, M. Alliance of atomic-scale/nanoscale Fe/Co active sites with hierarchically porous N-doped carbon frameworks for efficient electrocatalytic oxygen reduction. *Rare Met.* **2023**, *42* (11), 3766−3779.

(12) Liu, F.; Shan, W.; Lian, Z.; Liu, J.; He, H. The smart surface modification of Fe_2O_3 by WO_x for significantly promoting the selective catalytic reduction of NO with NH_3. *Appl. Catal., B* **2018**, *230*, 165−176.

(13) Chen, W.; Yang, S.; Liu, H.; Huang, F.; Shao, Q.; Liu, L.; Sun, J.; Sun, C.; Chen, D.; Dong, L. Single-atom Ce-modified α-Fe_2O_3 for selective catalytic reduction of NO with NH_3. *Environ. Sci. Technol.* **2022**, *56* (14), 10442−10453.

(14) Dong, S.; Wang, H.; Zhu, T.; Qu, Z. High-performance Fe-Cu composite oxide for selective catalytic reduction of NO with NH_3: driving of Cu on α-Fe_2O_3. *J. Environ. Chem. Eng.* **2022**, *10* (5), No. 108481.

(15) Lyu, Z.; Niu, S.; Lu, C.; Zhao, G.; Gong, Z.; Zhu, Y. A density functional theory study on the selective catalytic reduction of NO by NH_3 reactivity of α-Fe_2O_3 (001) catalyst doped by Mn, Ti, Cr and Ni. *Fuel* **2020**, *267*, No. 117147.
(16) Peng, Y.; Jiang, W.; Liu, Y.; Yao, L.; Chen, Y.; Yang, L. The multi-metal oxides blended activated coke for efficient NH_3-SCR at super low-temperature. *J. Environ. Chem. Eng.* **2022**, *10* (6), No. 108799.
(17) Yang, X.; Li, B.; Sun, L.; Huang, Z.; Cheng, X.; Zhang, T.; Tang, X. Effect of surface structure of α-Fe_2O_3 on the selective catalytic reduction of NO by NH_3. *Acta Phys. -Chim. Sin.* **2012**, *28* (01), 184−188.
(18) Mou, X.; Zhang, B.; Li, Y.; Yao, L.; Wei, X.; Su, D.; Shen, W. Rod-shaped Fe_2O_3 efficiently catalyzes selective reduction of nitrogen oxide by ammonia. *Angew. Chem., Int. Ed.* **2012**, *51* (12), 2989−2993.
(19) Ma, L.; Seo, C. Y.; Nahata, M.; Chen, X.; Li, J.; Schwank, J. W. Shape dependence and sulfate promotion of CeO_2 for selective catalytic reduction of NO with NH_3. *Appl. Catal., B* **2018**, *232*, 246−259.
(20) Zhu, L.; Yao, J.; Ma, G.; Cao, P.; Wu, S.; Li, Z. NH_3-SCR performance and SO_2 resistance comparison of CeO_2 based catalysts with Fe/Mo additive surface decoration. *Chem. Eng. J.* **2022**, *428*, No. 131372.
(21) Guo, M.; Liu, Q.; Zhao, P.; Han, J.; Li, X.; Ha, Y.; Fu, Z.; Song, C.; Ji, N.; Liu, C.; Ma, D.; Li, Z. Promotional effect of SO_2 on Cr_2O_3 catalysts for the marine NH_3-SCR reaction. *Chem. Eng. J.* **2019**, *361*, 830−838.
(22) Liu, F.; Asakura, K.; He, H.; Shan, W.; Shi, X.; Zhang, C. Influence of sulfation on iron titanate catalyst for the selective catalytic reduction of NO_x with NH_3. *Appl. Catal., B* **2011**, *103* (3−4), 369−377.
(23) Han, L.; Gao, M.; Feng, C.; Shi, L.; Zhang, D. Fe_2O_3-CeO_2@Al_2O_3 nanoarrays on Al-mesh as SO_2-tolerant monolith catalysts for NO_x reduction by NH_3. *Environ. Sci. Technol.* **2019**, *53* (10), 5946−5956.
(24) Zhang, Y.; Yang, S.; Zhu, X.; Xu, X.; Huang, F.; Yang, Z.; Sun, C. Effects of sulfation on hematite for selective catalytic reduction of nitrogen oxides with ammonia. *J. Colloid Interface Sci.* **2022**, *606*, 1445−1456.
(25) He, G.; Lian, Z.; Yu, Y.; Yang, Y.; Liu, K.; Shi, X.; Yan, Z.; Shan, W.; He, H. Polymeric vanadyl species determine the low-temperature activity of V-based catalysts for the SCR of NO_x with NH_3. *Sci. Adv.* **2018**, *4* (11), No. eaau4637.
(26) Yu, Y.; Tan, W.; An, D.; Wang, X.; Liu, A.; Zou, W.; Tang, C.; Ge, C.; Tong, Q.; Sun, J.; Dong, L. Insight into the SO_2 resistance mechanism on γ-Fe_2O_3 catalyst in NH_3-SCR reaction: a collaborated experimental and DFT study. *Appli. Catal., B* **2021**, *281*, No. 119544.
(27) An, D.; Yang, S.; Zou, W.; Sun, J.; Tan, W.; Ji, J.; Tong, Q.; Sun, C.; Li, D.; Dong, L. Unraveling the SO_2 poisoning effect over the lifetime of MeO_x (Me = Ce, Fe, Mn) catalysts in low-temperature NH_3-SCR: interaction of reaction atmosphere with surface species. *J. Phys. Chem. C* **2022**, *126* (29), 12168−12177.
(28) Gu, Z.; Cheng, L.; Tan, C.; Sin, S.; Huang, C.; Tang, C. Enriching SO_4^{2-} immobilization on α-Fe_2O_3 via spatial confinement for robust NH_3-SCR denitration. *Catalysts* **2022**, *12* (9), No. 991, DOI: 10.3390/catal12090991.
(29) Tan, W.; Wang, J.; Yu, S.; Liu, A.; Li, L.; Guo, K.; Luo, Y.; Xie, S.; Gao, F.; Liu, F.; Dong, L. Morphology-sensitive sulfation effect on ceria catalysts for NH_3-SCR. *Top. Catal.* **2020**, *63* (9−10), 932−943.
(30) Chen, J.; Zhao, W.; Wu, Q.; Mi, J.; Wang, X.; Ma, L.; Jiang, L.; Au, C.; Li, J. Effects of anaerobic SO_2 treatment on nano-CeO_2 of different morphologies for selective catalytic reduction of NO_x with NH_3. *Chem. Eng. J.* **2020**, *382*, No. 122910.
(31) Wu, C.; Yin, P.; Zhu, X.; OuYang, C.; Xie, Y. Synthesis of hematite (α-Fe_2O_3) nanorods: diameter-size and shape effects on their applications in magnetism, lithium ion battery, and gas sensors. *J. Phys. Chem. B* **2006**, *110* (36), 17806−17812.
(32) Liu, Z.; Su, H.; Chen, B.; Li, J.; Woo, S. I. Activity enhancement of WO_3 modified Fe_2O_3 catalyst for the selective catalytic reduction of NO by NH_3. *Chem. Eng. J.* **2016**, *299*, 255−262.
(33) Zhu, W.; Tang, X.; Gao, F.; Yi, H.; Zhang, R.; Wang, J.; Yang, C.; Ni, S. The effect of non-selective oxidation on the $Mn_2Co_1O_x$ catalysts for NH_3-SCR: positive and non-positive. *Chem. Eng. J.* **2020**, *385*, No. 123797.
(34) He, G.; Gao, M.; Peng, Y.; Yu, Y.; Shan, W.; He, H. Superior oxidative dehydrogenation performance toward NH_3 determines the excellent low-temperature NH_3-SCR Activity of Mn-based catalysts. *Environ. Sci. Technol.* **2021**, *55* (10), 6995−7003.
(35) Chen, L.; Yang, X.; Chen, J.; Liu, J.; Wu, H.; Zhan, H.; Liang, C.; Wu, M. Continuous shape- and spectroscopy-tuning of hematite nanocrystals. *Inorg. Chem.* **2010**, *49* (18), 8411−8420.
(36) Wang, H.; Jin, B.; Wang, H.; Ma, N.; Liu, W.; Weng, D.; Wu, X.; Liu, S. Study of Ag promoted Fe_2O_3@CeO_2 as superior soot oxidation catalysts: the role of Fe_2O_3 crystal plane and tandem oxygen delivery. *Appl. Catal., B* **2018**, *237*, 251−262.
(37) Gu, Z.; Tan, C.; Zhu, B.; Sin, S.; Ji, J.; Wang, Y.; Cheng, L.; Song, W.; Huang, C.; Tao, M.; Tang, C. SO_4^{2-} immobilization regulated by reaction atmosphere over ABS poisoned α-Fe_2O_3 catalysts for efficient NO_x removal. *Chem. Eng. J.* **2023**, *475*, No. 146336.
(38) Guivar, J. A. R.; Sanches, E. A.; Bruns, F.; Sadrollahi, E.; Morales, M. A.; López, E. O.; Litterst, F. J. Vacancy ordered γ-Fe2O3 nanoparticles functionalized with nanohydroxyapatite: XRD, FTIR, TEM, XPS and Mössbauer studies. *Appl. Surf. Sci.* **2016**, *389*, 721−734, DOI: 10.1016/j.apsusc.2016.07.157.
(39) Sun, C.; Liu, H.; Chen, W.; Chen, D.; Yu, S.; Liu, A.; Dong, L.; Feng, S. Insights into the Sm/Zr co-doping effects on N_2 selectivity and SO_2 resistance of a MnOx-TiO_2 catalyst for the NH_3-SCR reaction. *Chem. Eng. J.* **2018**, *347*, 27−40.
(40) Yao, X.; Kang, K.; Cao, J.; Chen, L.; Luo, W.; Zhao, W.; Rong, J.; Chen, Y. Enhancing the denitration performance and anti-K poisoning ability of CeO_2-TiO_2/P25 catalyst by H_2SO_4 pretreatment: structure-activity relationship and mechanism study. *Appl. Catal., B* **2020**, *269*, No. 118808.
(41) Gao, M.; He, G.; Zhang, W.; Du, J.; He, H. Reaction pathways of the selective catalytic reduction of NO with NH_3 on the α-Fe_2O_3 (012) Surface: a combined experimental and DFT study. *Environ. Sci. Technol.* **2021**, *55* (16), 10967−10974.
(42) Song, L.; Chao, J.; Fang, Y.; He, H.; Li, J.; Qiu, W.; Zhang, G. Promotion of ceria for decomposition of ammonia bisulfate over V_2O_5-MoO_3/TiO_2 catalyst for selective catalytic reduction. *Chem. Eng. J.* **2016**, *303*, 275−281.
(43) Cai, Y.; Zhang, B.; Yu, H.; Ji, X.; Sun, J.; Wang, X.; Qian, Q.; Li, L.; Liu, A.; Tan, W.; Gao, F.; Dong, L. Shielding ceria based catalysts from SO_2 poisoning in NH_3-SCR reaction: modification effect of acid metal oxides. *Appl. Catal., B* **2024**, *342*, No. 123424.
(44) Wang, X.; Du, X.; Liu, S.; Yang, G.; Chen, Y.; Zhang, L.; Tu, X. Understanding the deposition and reaction mechanism of ammonium bisulfate on a vanadia SCR catalyst: a combined DFT and experimental study. *Appli. Catal., B* **2020**, *260*, No. 118168.
(45) Yang, S.; Guo, Y.; Chang, H.; Ma, L.; Peng, Y.; Qu, Z.; Yan, N.; Wang, C.; Li, J. Novel effect of SO_2 on the SCR reaction over CeO_2: mechanism and significance. *Appl. Catal., B* **2013**, *136*−*137*, 19−28.
(46) Huang, H.; Lan, Y.; Shan, W.; Qi, F.; Xiong, S.; Liao, Y.; Fu, Y.; Yang, S. Effect of sulfation on the selective catalytic reduction of NO with NH_3 over γ-Fe_2O_3. *Catal. Lett.* **2014**, *144* (4), 578−584.
(47) Cai, Y.; Yang, P.; Liu, Q.; Ma, K.; Ma, W.; Song, W.; Qian, Q.; Gao, F.; Tan, W.; Dong, L. Getting insights into gas-phase sulfation effect on catalytic performance of praseodymium oxides in NH_3-SCR of NO. *J. Rare Earths* **2023**, *41* (6), 952−958.
(48) Guo, K.; Zhu, Y.; Yan, Z.; Liu, A.; Du, X.; Wang, X.; Tan, W.; Li, L.; Sun, J.; Tong, Q.; Tang, C.; Dong, L. The dual effects of ammonium bisulfate on the selective catalytic reduction of NO with NH_3 over Fe_2O_3-WO_3 catalyst confined in MCM-41. *Chem. Eng. J.* **2020**, *389*, No. 124271.

(49) Zhu, Z.; Niu, H.; Liu, Z.; Liu, S. Decomposition and reactivity of NH_4HSO_4 on V_2O_5/AC catalysts used for NO reduction with ammonia. *J. Catal.* **2000**, *195* (2), 268−278.
(50) Hu, W.; He, J.; Liu, X.; Yu, H.; Jia, X.; Yan, T.; Han, L.; Zhang, D. SO_2- and H_2O-tolerant catalytic reduction of NO_x at a low temperature via engineering polymeric VO_x species by CeO_2. *Environ. Sci. Technol.* **2022**, *56* (8), 5170−5178.
(51) Kijlstra, W. S.; Daamen, J. C. M. L.; van de Graaf, J. M.; van der Linden, B.; Poels, E. K.; Bliek, A. Inhibiting and deactivating effects of water on the selective catalytic reduction of nitric oxide with ammonia over MnO/Al_2O_3. *Appl. Catal., B* **1996**, *7* (3−4), 337−357.
(52) Liu, F.; He, H. Selective catalytic reduction of NO with NH_3 over manganese substituted iron titanate catalyst: reaction mechanism and H_2O/SO_2 inhibition mechanism study. *Catal. Today* **2010**, *153* (3−4), 70−76.
(53) Huang, Z.; Zhu, Z.; Liu, Z. Combined effect of H_2O and SO_2 on V_2O_5/AC catalysts for NO reduction with ammonia at lower temperatures. *Appl. Catal., B* **2002**, *39*, 361−368.
(54) He, S.; Ren, J.; Cao, P. Green Ce-based honeycomb catalyst with excellent water and sulfur dioxide resistances for low-temperature selective catalytic reduction of NO_x with ammonia. *Process Saf. Environ. Protect.* **2022**, *162*, 1−16.

https://doi.org/10.1021/acs.est.4c00276
Environ. Sci. Technol. 2024, 58, 8955−8965